

Check for updates

Original research article



Microstructure and mechanical properties of a novel Titanium-based alloy with high elastic strain for orthopedic implant applications

Materials Science and Technology I-17 © The Author(s) 2025 Article reuse guideline: sagepub.com/journals-permissions DOI: 10.1177/02670836251378798 journals.sagepub.com/home/mst



Arash Etemad¹, Alireza Mashreghi¹, Saeed Hasani¹, Sabine Schwarz² and Martin Lombaard³

Abstract

This study develops a biocompatible Ti-37.5Nb-4.5Zr alloy for orthopedic implants, addressing strength-ductility and stress shielding issues by leveraging twinning-induced plasticity (TWIP) and transformation-induced plasticity (TRIP) effects, and controlled phase transformations among β , ω , α' , and α'' phases with comprehensive characterization, such as CALPHAD, dilatometry, X-ray diffraction (XRD), transmission electron microscopy (TEM), and mechanical testing. Results show a cold-rolled sample with a yield strength of 1050 \pm 20 MPa, tensile strength of 1340 \pm 15 MPa, elastic modulus of 40.5 \pm 0.2 GPa, and 2.1 \pm 0.2% elongation, while the annealed sample at 700°C for 30 min achieve 750 \pm 10 MPa yield strength, 1050 \pm 10 MPa tensile strength, 44.0 \pm 0.4 GPa modulus, and 26.2 \pm 1.1% elongation, demonstrating a balanced combination of strength, ductility, and elastic strain suitable for advanced orthopedic applications.

Keywords

metastable β titanium alloys, biomedical materials, omega phase, deformation twinning, martensitic transformation

Received: 30 April 2025; accepted: 31 August 2025

Introduction

The application of thermo-mechanical processes through various routes leads to the formation of a wide range of microstructures in Ti-based alloys, resulting in different phase fractions, morphologies, and distributions, which ultimately changes their mechanical properties significantly. To address the inherent trade-off between strength and ductility in Ti-based alloys, the focus has shifted toward metastable β -Ti alloys that exhibit enhanced ductility mechanisms and excellent strain hardening capability, particularly in the last decade. ²

Average bond order (\overline{Bo}) -average d-orbital energy level (\overline{Md}) phase diagrams provide a promising approach for the design and development of Ti-based alloys. These diagrams are constructed using three overall electronic parameters, including the average electron/atom ratio (e/a), \overline{Bo} , and \overline{Md} have demonstrated significant potential in alloy design.³

On the other hand, the admissible elastic strain (δ) , calculated from the ratio of yield strength to Young's modulus (E), reflects an important combination of properties and serves as a key parameter for guiding material selection in biomedical applications.⁴ A higher admissible elastic strain indicates greater suitability for materials intended for biomedical implants.

The addition of Nb and Zr elements (both highly biocompatible metals⁴) into Ti-based alloys enables the creation of strong, lightweight, and durable alloys with low elastic moduli. This characteristic is crucial for orthopedic implants, as a

mismatch in the Young's modulus between the implant and surrounding bone can lead to complications referred to as "stress shielding".⁵

Numerous literature reviews have explored the thermomechanical processing, 6,7 microstructure-properties relationships, 8,9 and applications 10,11 of metastable β -Ti alloys. However, due to the high variety of achievable compositions in these alloys, identifying a composition that precisely meets desired requirements can be challenging.

To overcome the challenge of achieving both high strength and ductility in metastable β -Ti alloys, a combination of precipitation hardening with two phenomena, Twinning-Induced Plasticity (TWIP) and Transformation-Induced Plasticity (TRIP), can be utilized. Historically observed in steels, dynamic phase transformation and twinning during deformation concurrently enhance strength, ductility, and strain hardening. The family of strain-induced transformation TRIP/

Corresponding author:

Saeed Hasani, Department of Mining and Metallurgical Engineering, Yazd University, Yazd, Iran.
Email: hasani@yazd.ac.ir

Department of Mining and Metallurgical Engineering, Yazd University,

²University Service Centre for Transmission Electron Microscopy, Technische Universität Wien, Wien, Austria

³Anton Paar GmbH, Graz, Austria

TWIP Ti-based alloys has been developed over the last decade by strategically adding alloying elements to control the stability of the β phase. ^{13–15} The instability of the β phase makes it susceptible to transforming into twins and/or new phases, thereby inducing significant TWIP and/or TRIP effects. This deformation mechanism can lead to the formation of {112} and {332} twins, α'/α'' martensite, and the ω phase. ^{11,16} Notably, the interfaces formed, including twin boundaries and phase boundaries, act as strong and effective obstacles to dislocation slip.

The α'' phase has an orthorhombic crystal structure, whereas the α' phase exhibits a hexagonal crystal structure. Both the α' and α'' phases predominantly form through stress-induced transformation from the β phase or during the quenching process in titanium-niobium alloys. This transformation is primarily driven by lattice changes occurring near twin boundaries. ¹⁶

The transition from the β to ω phase (as a hexagonal phase) can occur through two primary routes: (i) rapid cooling from the single β phase field at high temperature or subsequent isothermal aging, resulting in the formation of ellipsoidal or cuboidal ω particles homogeneously distributed throughout the β matrix, or (ii) compressive loading at a high strain rate (or shock loading), resulting in ω plates with a heterogeneous distribution, generally located along $\{112\}$ or $\{332\}$ twin boundaries.

Although the influence of the ω phase on the mechanical properties of metastable β -Ti-based alloys has been explored, these investigations have largely struggled to maintain ductility. It is critical to note that the precipitation of secondary phases (α and/or ω) may influence the affects of TWIP and TRIP. Therefore, systematic research is needed to integrate ω phase precipitation with TRIP/TWIP effects to thoroughly understand their combined influence on strength and ductility. Hence, this paper aims to design and produce a new biocompatible alloy, focusing on the interaction of four phases (α' , α'' , ω , and β) and their effect on deformation mechanisms and mechanical properties.

Materials and methods

Sample production

The ingots with a nominal composition of Ti-37.5Nb-4.5Zr (wt.%) were prepared using vacuum arc melting (VAR, FZKH-100VAR-L, Farazob Khala, Tehran, Iran) in a water-cooled copper crucible under a high-purity argon atmosphere. High-purity Ti (99.999 wt%), Nb (99.95 wt%), and Zr (99.95 wt%) were utilized as starting materials. To improve homogeneity, the ingots were remelted at least six times, with the ingot being turned over between each melting cycle. The chemical composition was confirmed using inductively coupled plasma-optical emission spectrometry (ICP-OES, Leco ONH836, Michigan, USA) analysis. The results, detailed in Table 1, showcase a close alignment with the target composition.

The ingots were then homogenized under vacuum in a quartz tube along with a pure Ti getter at 1100°C for 2 h and subsequently quenched in ice water. After it, the

Table 1. Chemical composition of the investigated alloy.

Element	Nb	Zr	Fe	0	Ti
Amount (wt.%)	39.6	4.3	0.2	0.002	Bal.

homogenized ingots were hot-rolled at 950°C to produce a plate with a thickness of 4.5 mm, achieving a total thickness reduction of approximately 75%. After removing the oxide layer, the ingots were cold-rolled at room temperature, achieving a total reduction of approximately 95% without intermediate annealing. Finally, the cold-rolled samples were annealed at temperatures of 400, 500, 600, 700, 800, 850, 900, and 1000°C for 30 min under vacuum, followed by quenching in ice water.

Characterization

CALPHAD calculations were performed using Thermo-Calc software, incorporating the TCHEA6 database along with the upgraded TCFE9 databases.

Cylindrical samples (4 mm diameter, 25 mm height) were prepared by electrical discharge machining (EDM) for dilatometry testing. The tests were performed using a DIL 805 A/D apparatus (TA Instruments, New Castle, USA) at heating and cooling rate of 5 K/min, reaching temperatures up to 1400°C. Also, the phase evolutions of the annealed samples was analyzed through X-ray diffraction (XRD) using an Asenware AW-DX300 diffractometer (Beijing, China) with Cu Kα radiation (30 mA, 40 kV). Scans were performed from 20 to 100° in 2 θ , with step size of 0.05 $^{\circ}$ and step times of 1 s. Furthermore, high temperature X-ray diffraction (HT-XRD) patterns of the homogenized sample were recorded between 20 and 100° at different temperatures (200, 400, 1100, 1400°C). HT-XRD was performed on an Anton-Paar XRDynamic 500 (Graz, Austria) using a Primux 3000 Cu source operating at 40 kV. The nominal heating rate was set at 20°C/min, with a scan time was 59 min and a step size of 0.01°.

For tensile tests, the oriented rolling direction plate-type and sub-sized tensile specimens (3 mm wide, 15 mm long) were fabricated from the annealed samples using EDM. These tests were performed at a strain rate of 10^{-3} 1/s using a Santam 15 Ton universal testing machine (Tehran, Iran) and the tests were repeated three times for each specimen. Also, Vickers microhardness testing was performed on the samples at room temperature using a 200 g load and a 10 s dwell time with a (Buehler, Micromet 5101, Illinois, USA). Five measurements were taken on each sample, and the average hardness value was reported.

Microstructural features of the hot-rolled, cold-rolled, and annealed samples were examined in the rolling direction (RD)-transverse direction (TD) plane using transmission electron microscopy (TEM) with a 200 kV FEI TECNAI F20 S-Twin (Massachusetts, USA). TEM samples were prepared through cutting, grinding, and subsequent twin-jet electropolishing at -35°C in an electrolyte composed of 60 vol% methanol, 5 vol% perchloric acid, and 35 vol% 2-butoxyethanol.

Results and discussion

Design of metastable β -Titanium alloys

A critical characteristic of metastable β -titanium alloys is the stability of β phase, which is directly related to its composition. β phase stability is of paramount importance because its significantly influences the martensitic transformation and the amount of martensite formation under both thermal (e.g., quenching) and stress-induced conditions. The β -phase composition strongly affects stress-induced martensite, and is closely associated with the Ms temperature. ^{17,18} Furthermore, the deformation mechanisms in these alloys also dependent on β -phase stability. ^{18–20}

Stable β titanium alloys typically undergo plastic deformation through a slip-dominated mechanism. This mechanism, characterized by localized strain concentration, often results in limited ductility. ^{18–21} In a stable β matrix, plastic deformation is primarily driven by the activation of slip dislocations, with shear bands becoming the dominant mechanism at later stages.

As the β -phase stability of titanium alloys decreases, the deformation mechanism tends to shift towards $\{112\}\langle111\rangle$ twinning, $\{332\}\langle113\rangle$ twinning systems, and stress-induced martensitic transformations ($\beta \to \alpha$ " and $\beta \to \omega$). Research indicated that activating multiple deformation mechanisms can significantly improve the ductility limitations associated with slip-dominated deformation. ^{18,22,23}

Consequently, tailoring the β -phase stability, and consequently the deformation mechanisms, has emerged as a crucial strategy in designing metastable β -titanium alloys. This highlights the necessity for accurately estimating β -phase stability, particularly when developing more practical metastable β -titanium alloys.

The molybdenum equivalence (Mo_{eq}) is the most widely used method for evaluating and quantifying β -phase stability in titanium alloys. It is calculated as a linear sum of the weight percentages of the constituent alloying elements, as presented in Eq. (1):²⁴

$$\begin{split} \text{Mo}_{\text{eq}} = & 1.0 (\text{wt.\%Mo}) + 0.67 (\text{wt.\%V}) + 0.44 (\text{wt.\%W}) \\ & + 0.28 (\text{wt.\%Nb}) + 0.22 (\text{wt.\%Ta}) + 2.9 (\text{wt.\%Fe}) \\ & + 1.6 (\text{wt.\%Cr}) + 1.25 (\text{wt.\%Ni}) + 1.70 (\text{wt.\%Mn}) \\ & + 1.70 (\text{wt.\%Co}) - 1.0 (\text{wt.\%Al}) \end{split}$$

In contrast, aluminum (Al) is not included in the equation, as it promotes α -phase stabilization, as previously discussed.

(1)

$$Al_{E} = 1.0(wt.\%Al) + 0.17(wt.\%Zr) + 0.33(wt.\%Sn) + 10(wt.\%O)$$
(2)

This highlights that the each constituent element has a distinct influence on phase stability within Ti alloys. A Mo_{eq} of 10.0 typically stabilizes the β -phase upon quenching, with higher Mo_{eq} values corresponding to lower T_{β} temperatures. A high Mo_{eq} value suggests a high degree of β -phase stability, a phenomenon commonly observed in multicomponent alloy systems. Neelakantan et al. ²³ presented a linear relationship between the M_s temperature and the compositional

characteristics of the β -phase, quantified in wt%:

$$M_s = 1156-150$$
Fe-107Mn-96Cr-67Ni-49Mo-41Cu-37V
-17Nb-7Zr + 15Al

(3)

Therefore, in-situ β -phase composition acts as the independent variable in the relationships expressed by Eqs. (1) and (3), which predict β -phase stability and M_s temperature, respectively. More importantly, this is highly useful for predicting or designing alloy compositions, that is, the more stable the β -phase, the lower the M_s temperature. Consequently, increased β -phase stability correlates with a decreased M_s temperature.

In the DV-X α cluster method, a general approach for evaluating the phase stability and elastic properties of β -Ti alloy by Abdel-Hady et al., ²⁵ two parameters-bond order (\overline{Bo}) and metal d-orbital energy level (\overline{Md}) -are used to define the martensitic and omega transformation boundaries in relation to the β -phase modulus. \overline{Bo} quantifies the strength of the chemical bond between Ti and the alloying elements. \overline{Md} derived from the alloying element's electronegativity and metallic radius, reflects its electronic properties. ²⁶ For the alloys under consideration, the average values of \overline{Bo} and \overline{Md} are provided in references. ^{27,28} Additionally, the electron-to-atom ratio (e/a), as an important electronic indicator, affects the stability of the β phase and its transformation boundaries.

$$\overline{Bo} = \sum_{i=1}^{n} x_i (Bo)_i \tag{4}$$

$$\overline{Md} = \sum_{i=1}^{n} x_i (Md)_i \tag{5}$$

$$\overline{e/a} = \sum_{i}^{n} x_i e_i \tag{6}$$

For each alloying element i, x_i denotes its atomic fraction, while $(Bo)_i$ and $(Md)_i$ represent its bond order and metal d-orbital energy level, respectively, where e_i is the valence number of the ith atom. In addition, the phase stability map can be constructed using \overline{Bo} and \overline{Md} , as initially proposed by Morinaga et al.²⁹ The position of a designed alloy on this phase stability map is determined by its chemical composition.

The Young's modulus along the $\beta/(\beta + \omega)$ phase boundary decreases with increasing values of \overline{Bo} and \overline{Md} .^{4,25} The minimum Young's modulus is observed in an alloy with an e/a ratio between 4.07 and 4.20, where the metastable β phase and α'' and/or α' phases can be formed at room temperature.³⁰ It was experimentally found that a lower e/a ratio correlates with a decrease in the elastic modulus of metastable β -type titanium alloys.⁵

Two groups of metastable β -type titanium alloys have been developed that balance high strength with low elastic modulus. One group, known as Gum Metal, has an e/a ratio of approximately 4.24, ^{31,32} which is suitable for biomedical titanium alloys due to its low elastic modulus. The other

alloy, Ti-24Nb-4Zr-8Sn (in wt%), has an *e/a* ratio of about 4.15.³³ Despite significant differences in composition and processing, both alloys exhibit unique non-linear tensile deformation behavior and highly localized plasticity. ^{31–33}

At an e/a ratio of 4.24, the Young's modulus in the {100} direction of the bcc structure approaches zero, indicating very high ductility in this direction. In addition to the low Young's modulus, the shear modulus in this direction is also significantly reduced, resulting in the lowest overall Young's modulus for the material. The work hardening ratio reaches its minimum value at an e/a ratio of 4.24, suggesting that candidate alloys should aim for this value or something close to it. 34,35

Furthermore, when the bond value is 2.87, both the elastic modulus and work hardening ratio reach their minimum. For the alloy to remain stable in the metastable beta phase, the \overline{Md} value should be approximately 2.45. 25,36

The \overline{Bo} and \overline{Md} diagram serves as a predictive tool that links β -phase chemical stability to the operative deformation mechanisms. Empirical validation across diverse alloy systems² confirms the diagram's effectiveness in predicting dominant deformation modes, including those induced by mechanical twinning. ^{26,37} Consequently, the \overline{Bo} and \overline{Md} phase stability diagram is a valuable tool for investigating how alloy composition-and, therefore, β -Ti phase stability-affects plastic deformation behavior.

Although the transition boundaries between different plasticity states are semi-empirically estimated based on a summary of experimental results, alloys situated near the transition lines on the \overline{Bo} and \overline{Md} map may exhibit a combination of plasticity states, such as TWIP and TRIP. Numerous successful cases have demonstrated the design of new metastable β -Ti alloys using the \overline{Bo} and \overline{Md} approach in open studies.²

However, recent research has revealed inaccuracies in the \overline{Bo} and \overline{Md} diagram's estimations of phase stability and deformation mechanisms when applied to specific metastable titanium alloys. A notable limitation is that the \overline{Bo} and \overline{Md} map does not account for mechanical strength. Additionally, the calculations for the \overline{Bo} and \overline{Md} exclude oxygen.

An example of the discrepancy between prediction and observation is observed in the Ti-10V-3Fe-3Al (wt.%) alloy. While the \overline{Bo} and \overline{Md} diagram indicated twinning, cold deformation resulted in the formation of stress-induced martensitic (α'') phase, ^{38,39} suggesting a potential inaccuracy in the diagram's predictive capabilities.

To address the limitations of existing models, Wang et al. ²⁸ introduced a semi-empirical method for evaluating the impact of deformation behavior on β -phase stability in Ti alloys. This new method incorporates the e/a and the atomic radius difference (Δr) , resulting in the e/a- Δr map.

$$\overline{\Delta r} = \sum_{i}^{n} c_i (r_i - r_{Ti}) \tag{7}$$

The e/a- Δr map displays the following characteristics:

 Higher e/a values are associated with slip-dominated deformation, whereas twinning and Stress-Induced Martensite (SIM) transformations are favored at e/a <4.2 and Δr>-2.5.

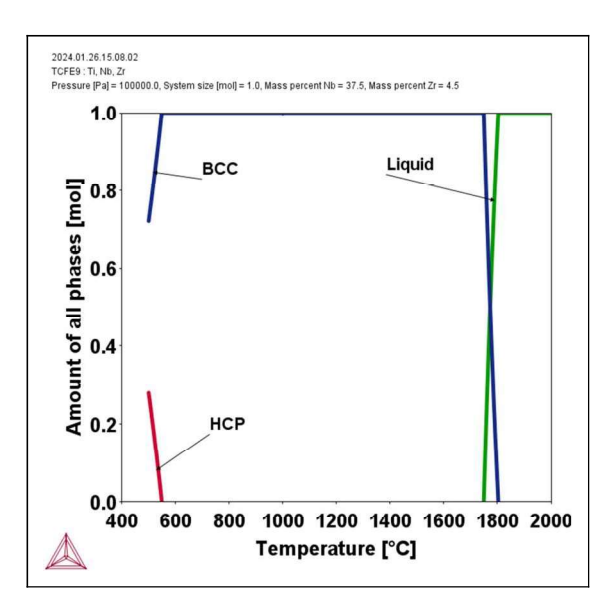


Figure 1. The calculated isopleth phase diagram of Ti-Nb-Zr system using Thermo-Calc's.

• The critical e/a value for the onset of twinning/SIM exhibits a maximum near $\Delta r = 0$ before decreasing as Δr increases.

As a result, with increased β -phase stability, both e/a and Δr influence lattice shear resistance, thereby affecting the deformation mechanisms in β -phase titanium alloys. Based on the design, the alloy was computed to have the following values:

- $\overline{Md} = 2.45$
- $\overline{Bo} = 2.87$
- e/a = 4.24
- $Mo_{eq} = 10.42$
- $\Delta r = 0.377$

One of the notable capabilities of Thermo-Calc's is its ability to identify and understand metastable phase transformations in Ti-based alloys, particularly Ti-Nb-Zr alloys. These transformations, often unexplainable by stable phase diagrams, are facilitated by Thermo-Calc's advanced modeling. ^{39–41}

In enhancing alloy performance for specific applications, such as dental and orthopedic implants, Thermo-Calc's plays a crucial role by the optimizing thermomechanical processing parameters. 42,43

The calculated phase diagram effectively illustrates the phase behavior of this alloy at various temperatures, as shown in Figure 1. The diagram clearly depicts the presence of HCP, BCC, and liquid phases, along with the transformations between them. At lower temperatures (below approximately 600°C), the HCP phase, also known as the ω phase is present, although its fraction gradually decreases with increasing temperature. As the temperature rises, the HCP phase progressively transforms into the BCC, and above 600°C, all HCP converts to BCC. The BCC phase remains the sole stable phase up to approximately 1600°C.

Literature indicates that the presence of Nb and Zr promotes the formation of the HCP phase in Ti-based alloys.

Zr with its relatively large atomic radius, is beneficial for both precipitation hardening and solid solution strengthening. ^{38,44,45}

Experimental results have shown that the phases observed at room temperature were formed due to the rapid cooling from higher temperatures, resulting in metastable phases.⁴² The phase compositions of the produced alloys were in satisfactory agreement with CALPHAD calculations.

Dilatometric test and phase analysis

The heating process induces the $\alpha+\beta\to\beta$ phase transformation, where the α phase (including α' and α'' phases) transforms into the β phase. The initial transformation temperature (T_s) and the final transformation temperature (T_f) are key parameters for characterizing the material's response to thermal conditions. The $\alpha+\beta\to\beta$ transformation typically begins around 720°C and completes by 950°C, as observed in similar titanium alloys.

The addition of Zr to Ti-Nb-based alloys lowers the peak temperature of the reverse martensitic transformation, thereby enhancing the stability of the martensitic phase. This indicates that adding Zr has a more significant effect on stabilizing the martensite phase than on reducing the peak temperature of the martensitic transformation. The dilatometric technique reveals the kinetics of phase transformations, showing an S-shaped pattern in the heating curve (as seen in Figure 2), indicative of the complex nature of the α to β transformation.

In Figure 2(b), within the temperature range of 1200 to 1300°C, a phase transformation peak occurs. This peak is characterized by two points: T_s , the start temperature of transformation at approximately 1199.3°C, and T_f ; the finishing temperature of transformation at around 1305.5°C. Between T_s and T_f ; the α phase (including α' and α'' phases) gradually dissolves into the β phase, resulting in a final microstructure composed entirely of the β phase.

On other hand, during cooling, especially in metastable β -Ti based alloys, the formation of the ω (HCP) phase is observed, as predicted by Thermo-Calc and observed in Figure 2(c). This phase typically forms during aging at intermediate temperatures, generally between 300 and 500°C in the β region (specifically around 489 to 495°C), and during slow cooling, characteristic of the ω_{iso} type. This process is diffusion-controlled and time-dependent; at intermediate temperatures, atoms have sufficient time for diffusion and rearrangement. The diffusion of alloying elements (such as Nb and Zr) leads to regions within the β matrix becoming enriched or depleted in these elements. Regions enriched with alloying elements are susceptible to the formation of this type of ω phase. ⁵⁰

It has been found that transformation temperatures decrease with increasing cooling rate, so the higher the cooling rate, the more rapid the phase transformation.⁵¹ The α' , α'' , and ω phases can form from the β phase during cooling, with the transformation temperature and rate being influenced by the cooling rate.^{44,52}

The interactions between these phases and their relative fractions are strongly dependent on the cooling rate, with faster cooling rates generally favoring the formation of α' and α'' phases over the β phase.⁴⁴ Due to the slow cooling rate of 5 K/min used in the dilatometry test, only the ω_{iso} phase is

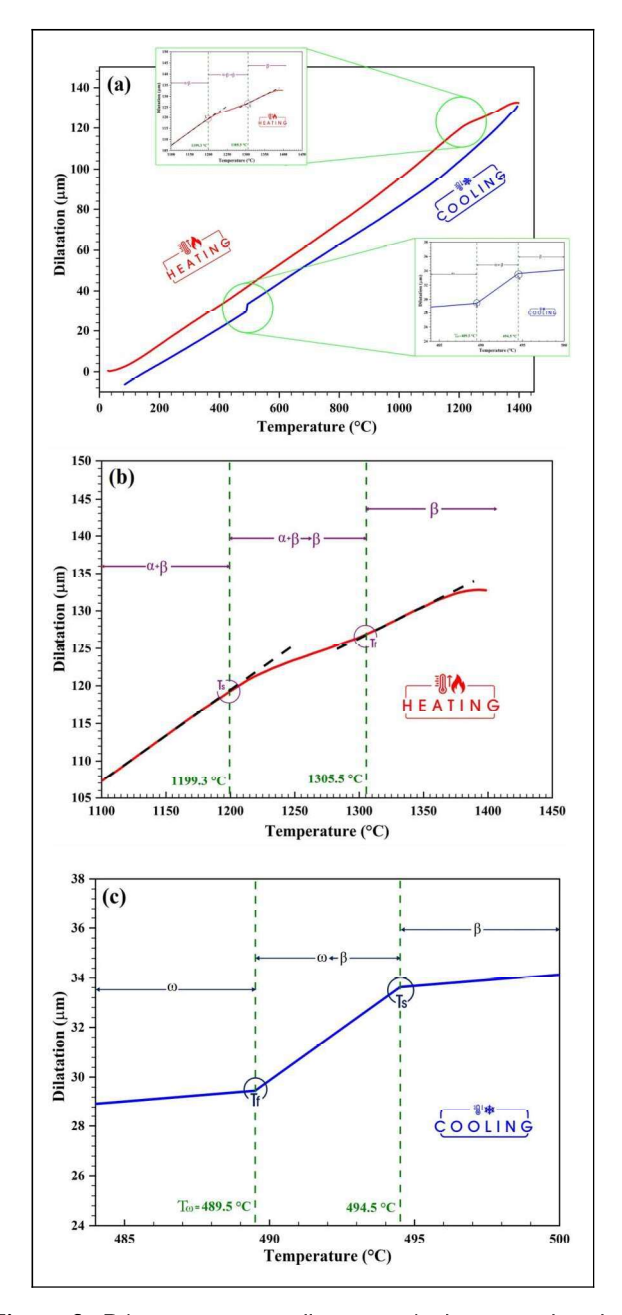


Figure 2. Dilatometry curves illustrating the heating and cooling rates for (a) Ti-37.5Nb-4.5Zr (wt.%) alloy at 5 K/min, (b) a detailed view of the starting and finishing temperatures of the $\alpha+\beta\to\beta$ phase transformation during the heating cycle, and (c) a detailed view of the starting and finishing temperatures of $\beta\to\omega$ phase transformation during the cooling cycle.

formed, while the α' and α'' phases are not appear. During heating, because the dilatometry test sample, which was homogenized and then quickly quenched in ice water after homogenization, contains a minor fraction of α' , α'' , and ω_{ath} (athermal type) phases. Upon heating the sample, ω_{ath} dissolves and allowing the β phase to grow. 53–55

In other words, the ω_{ath} phase forms during rapid cooling from the β region to lower temperatures; it is a non-equilibrium phase arising from high cooling rates. Its formation is diffusionless and exhibits a martensitic nature; meaning that atoms move collectively without the need for long-range diffusion. The instability of the beta phase lattice at lower temperatures causes the β (BCC) crystal structure to

transform into the ω (HCP) phase structure through a shear mechanism, and this transformation occurs very rapidly.

In-situ high-temperature X-ray diffraction (In-situ HT-XRD)

A previously homogenized sample (1100°C for 2 h, followed by ice-water quenching) was initially analyzed using in-situ high-temperature X-ray diffraction (HT-XRD) at room temperature. Phase analysis revealed the presence of β and ω phases (Figure 3(a)). The sample was then heated to 200°C and held at this temperature. At this point, the Ti₂ZrO phase appeared alongside the β and ω phases. Subsequently, in addition to the $\beta + \omega$ phases, the Ti₂ZrO phase appears, which can be considered a more complex oxide compared to simple oxides TiO₂ or ZrO₂ (Figure 3(b)). The formation of Ti₂ZrO indicates a combined oxidation behavior of Ti and Zr. This phase is commonly observed to nucleate during solidification, or more accurately, at lower thermal regimes, with its formation being contingent upon the oxygen concentration and potentially leading to interstitial solid solution strengthening. 52,56-58

When the temperature was increased to 400° C, the TiO_2 phase also appeared (Figure 3(c)). TiO_2 is typically observed as a secondary phase that can enhanced hardness but may also reduce ductility due to its brittle nature, especially along grain boundaries. ^{58,59} It is the primary oxide formed at lower temperatures and in the early stages of oxidation.

Upon further heating to 1100°C and holding it there, the TiNb_2O_7 phase emerged with significant intensity, in addition to the previously mentioned three phases (Figure 3(d)). TiNb_2O_7 is a ternary oxide composed of titanium, niobium, and oxygen, which can formed during high-temperature processing and is associated with improved mechanical properties due to its stable structure. The formation of TiNb_2O_7 indicates a more advanced stage of oxidation or specific conditions that favor the development of this ternary oxide.

As the temperature was raised to 1400° C, the intensity of these oxide phases decreases, because they are approaching their melting points^{56,57} (Figure 3(e)). After cooling the sample in the furnace and performing phase analysis again, the phases TiNb₂O₇, Ti₂ZrO, and $\beta + \omega$ were again observed, similar to those at 1100 and 1400°C (Figure 3(f)). Following sandpaper treatment to remove the oxide layers and subsequent phase analysis, the β and ω phases, along with minor volume fraction of the oxide phases TiNb₂O₇ and TiO₂, are detected (Figure 3(g)).

The oxidation process in this alloy begins with the diffusion of oxygen atoms from the surface into the interior. It is hypothesized that oxygen diffusion occurs preferentially, suggesting that oxygen transport may vary across the different phases due to differences in crystal structure and activation energy for diffusion within the β and ω phases.

The kinetics of oxide formation exhibits strong temperature dependence. At lower temperatures, the rates of oxygen diffusion and associated chemical reactions leading to a slower rate of oxide formation. Conversely, as the temperature increases, both diffusion and reaction rates accelerate, resulting in a higher rate of oxide formation. The oxidation

process proceeds in a stepwise manner: at lower temperatures, simpler oxides like TiO₂ and mixed oxides such as Ti₂ZrO are preferentially formed. At elevated temperatures, more complex oxides, such as TiNb₂O₇, emerge. This sequential phase evolution clearly demonstrates that the kinetics of phase formation are modulated by temperature.⁶¹

Phase and structural analysis

XRD and TEM studies on the Ti-37.5Nb-4.5Zr (wt.%) alloy revealed significant phase transformations under various processing conditions. These transformations were examined in the as-cast, homogenized, hot rolled (75% area reduction), cold rolled (95% area reduction), and heat-treated states at different temperatures, and are discussed in detail in the following sections.

As-cast and homogenized states: Initial β phase structure. In the as-cast and homogenized alloy samples, the X-ray Diffraction (XRD) results, as shown in Figure 4, indicate that the β phase is dominant phase in the structure. Under these conditions, the alloy primarily consists of the stable β phase, which is thermodynamically favored at high temperatures. This stability can be attributed to the nature of the Ti-Nb-Zr alloys and the presence of β -phase stabilizers, particularly Nb, known for its strong β -phase stabilization in Ti-systems.

High temperatures during casting and homogenization ensure that the β -phase remains the most stable phase. Furthermore, the homogenization and quenching heat treatment eliminate structural inhomogeneities, improving the distribution of alloying elements and resulting in a more uniform microstructure of equiaxed β grains. This process enhances the stability of the β phase further.

The ω phase is distributed as the fine and uniform particles dispersed throughout the β phase matrix (Figure 5(a)). The formation of the ω phase during cooling from high temperatures, such as the casting temperature, can be attributed to the characteristics of its phase transformation. The $\beta \to \omega$ transformation occurs via a displacive mechanism, which does not require long-range atomic diffusion and can occur during rapid cooling.

The presence of fine, homogeneously dispersed ω particles indicates that the formation of the ω phase in the β matrix follows a mechanism of homogeneous nucleation and growth. XRD studies reveal that the ω phase forms as coherent precipitates with a hexagonal structure due to the periodic collapse of {111} planes in the β phase. ^{62,63} Figure 5(b) shows selected area electron diffraction (SAED) pattern which reveals the presence of two distinct phases: the matrix phase with a body-centered cubic (BCC) crystal structure of β -Ti type with space group im3~m, and a secondary ω phase. The pattern originating from the matrix phase with a zone axis of [111] and the pattern of the ω phase with a zone axis of [21 $\overline{3}$ 1] are simultaneously observed in this image, indicating the coexistence of these two phases in the selected area of the sample.

The presence of secondary phases such as ω can induce structural changes in the alloy. For instance, broadening of XRD peaks indicates an increase in lattice defects and microstrains. In Ti-Nb-Zr alloys, the presence of the ω phase can

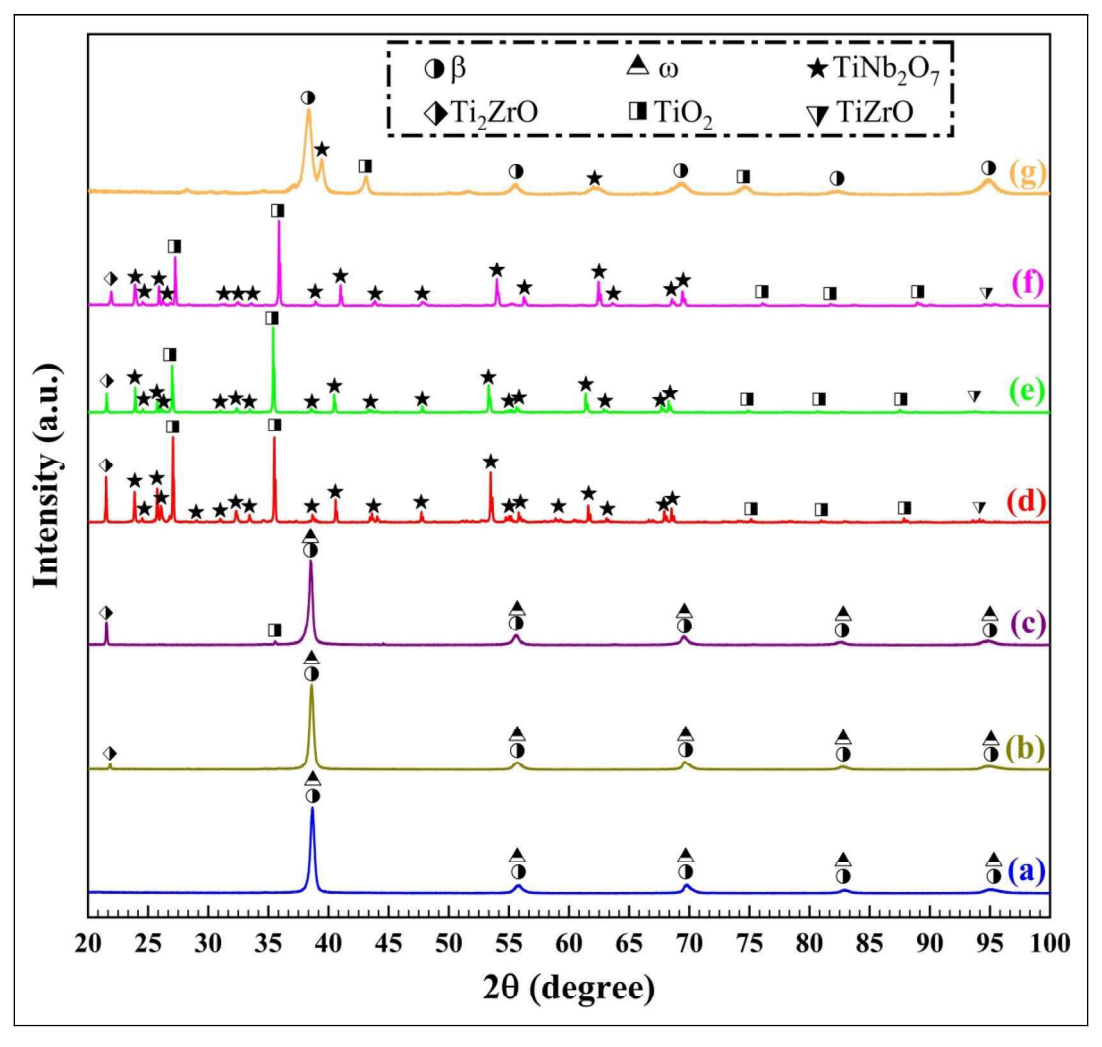


Figure 3. In-situ HT-XRD patterns of the Ti-37.5Nb-4.5Zr (wt.%) alloy at various temperatures: (a) room temperature, (b) 200, (c) 400, (d) 1100, and (e) 1400°C, (f) phase analysis after cooling in the furnace, and (g) phase analysis after removing oxide layers.

lead to a finer grain microstructure, thereby enhancing hardness and toughness.

Furthermore, the thermal stability of the ω phase improves with higher Nb concentration in the alloy, and lower stacking fault energy (SFE) promotes its formation. The $\beta \to \omega$ transformation can also occur due to severe plastic deformation, such as cold rolling, which induces compressive stress in the material. The ω phase can stabilize interfaces between different transformed phases, contributing to the structural integrity of the alloy. ^{64–66}

Accurately distinguishing between the β and ω phases in XRD patterns poses challenges due to their structural similarities and overlapping diffraction peaks. Additionally, the stability of the β phase at high temperatures, combined with the specific alloy composition, results in minimal formation of α' and α'' phases in the initial structure. When, they do form, the quantities are very low, and they do not produce distinguishable peaks in XRD patterns. The α' and α'' phases are martensitic, formed from the shear transformation of the β phase during rapid cooling, typically occurring in β alloys with lower β phase stability. In the as-cast and homogenized states, the high stability of the β phase (due to alloy composition and elevated temperature) significantly reduces the likelihood of martensitic transformation from β to α'/α'' , resulting in the absence of distinguishable peaks from these

phases in XRD. Consequently, no distinguishable peaks from these phases are observed in XRD. It is also noteworthy that the presence of oxygen in the structure can hinder the formation of ω and α'' phases after the cooling.⁴⁵

Effect of rolling processes (hot and cold): Induction of martensitic transformation. Rolling processes, particularly cold rolling, induces significant phase transformations in the alloy. In hot-rolled and especially cold-rolled samples, peaks corresponding to the martensitic α' and α'' phases appear alongside the β phase peaks. This indicates the transformation of the β phase into non-equilibrium martensitic α''/α' phases due to the thermomechanical effects of rolling. 67,68

Cold rolling imparts substantial plastic strain to the alloy, reducing the stability of the β phase and facilitating the martensitic transformation from β to α'/α'' . This transformation is referred to as SIM. As seen in Figure 6, in the investigated alloy, three distinct types of SIM: SIM α' , SIM α'' , and SIM ω are observed.

The dominant mechanism governing the deformation of metastable β titanium alloys includes dislocation slip, mechanical twinning, and phase transformation induced by stress or strain. The applied strain energy provides the activation energy necessary for the shear transformation, accelerating the formation of α' and α'' phases. The introduction of

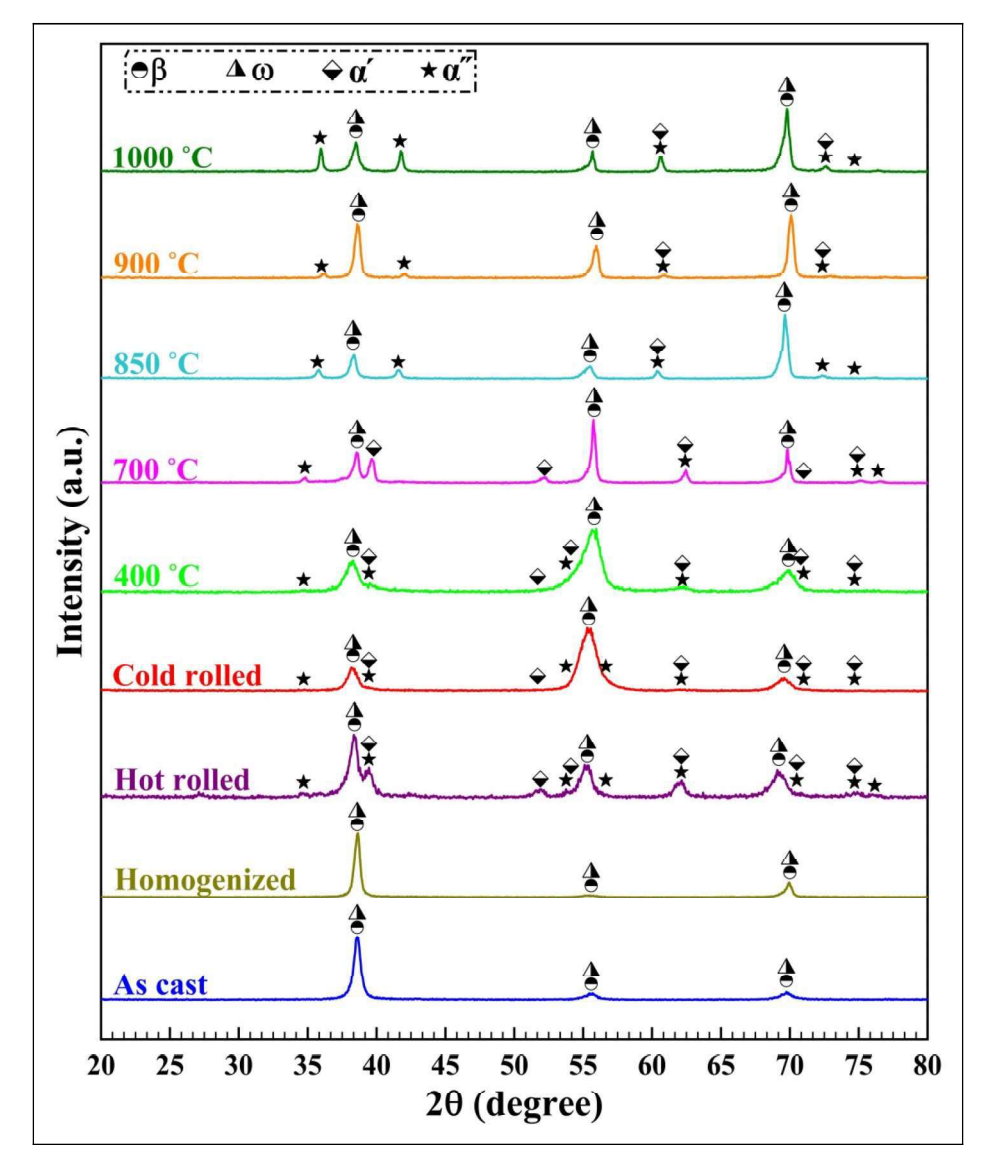


Figure 4. XRD patterns of the Ti-37.5Nb-4.5Zr (wt.%) alloy samples in various states: as-cast, homogenized, hot rolled, cold rolled, and annealed at 400, 700, 850, 900, and 1000°C.

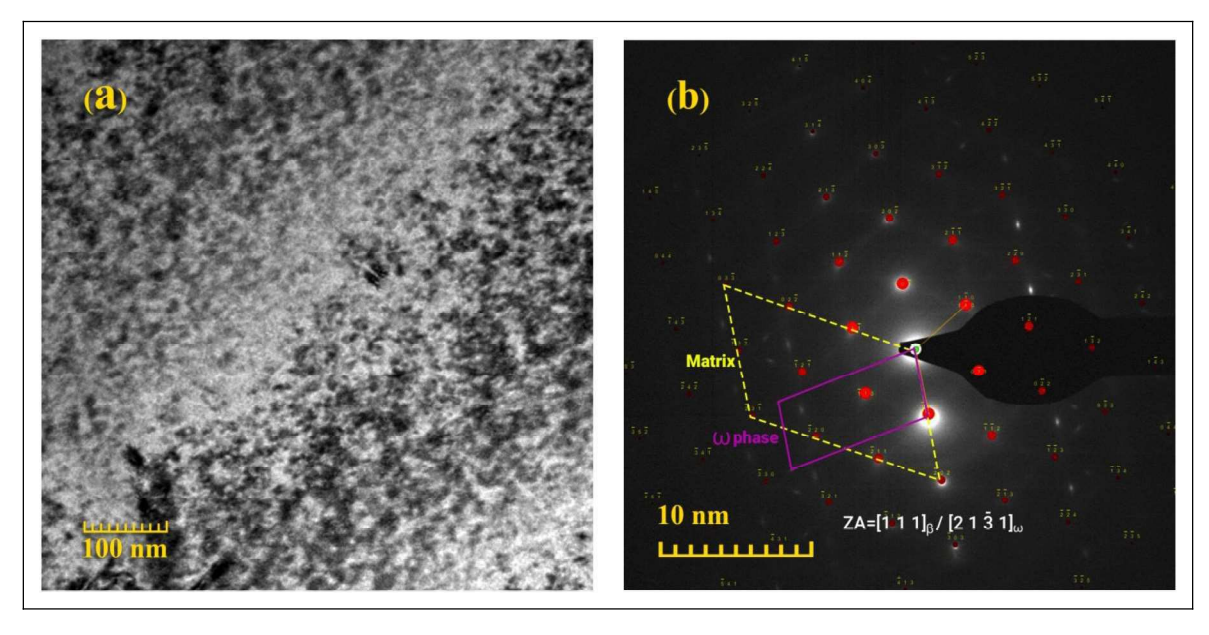


Figure 5. (a) Bright-field TEM image of the ω phase in the Ti-37.5Nb-4.5Zr (wt.%) alloy after homogenization and water quenching, and (b) selected area electron diffraction (SAED) patterns corresponding to the bright-field TEM image.

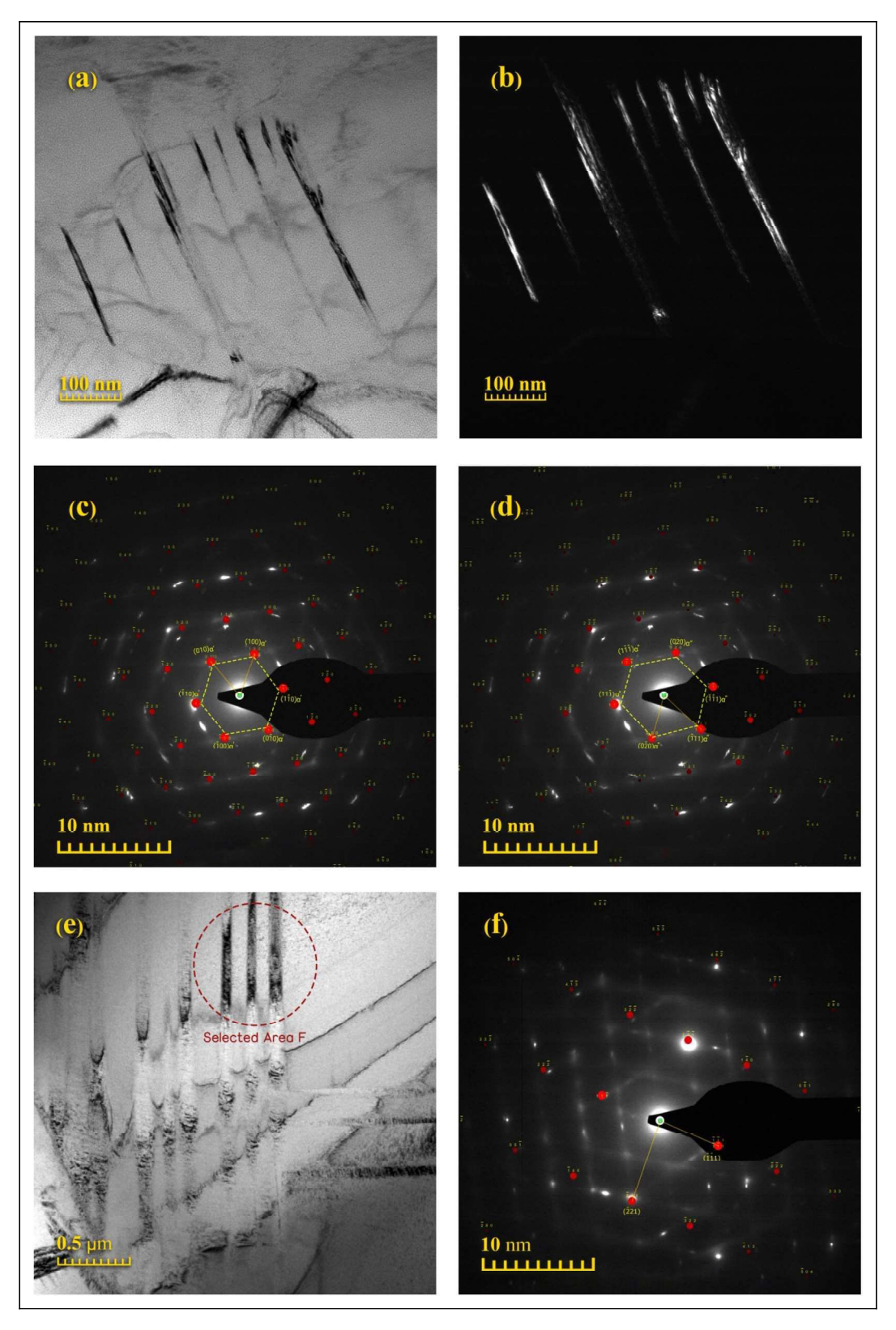


Figure 6. TEM image revealing SIM transformations in cold-rolled Ti-37.5Nb-4.5Zr alloy; (a) bright field (BF) image, (b) dark field (DF) TEM image of SIM α' and SIM α'' , (c) and (d) corresponding SAED patterns presented alongside the image to confirm their crystallographic structures and aid in phase identification, (e) BF image of SIM ω , and (f) SAED pattern of (e).

dislocations during deformation also promotes martensitic transformation, enabling the material to adapt to stress changes. The degree of strain-induced martensitic transformation correlates with the magnitude of applied plastic strain, with cold rolling typically introducing much higher plastic strains than hot rolling. Consequently, cold rolling drives

the transformation from β to α'/α'' more extensively, resulting in a higher volume fraction of these phases in the structure

During strain application, the softer β phase initially accommodates strain, followed by the the α'' phase and its interface with the matrix taking over strain accommodation.

This sequential activation facilitates the operation of various slip systems during deformation. After elongation to the alloy, thick deformation bands alongside narrow dislocation slip lines and twinning were observed, confirming that dislocation slip following quenching is the primary deformation mechanism in these alloys. The alloy structure allows for the activation of 48 different slip systems, with at least two separate slip systems being simultaneously activated within each grain. The dominant mobile dislocations in this system are edge dislocations of the type $\{110\}$ β <111> β .

Investigation of heat treatments at different temperatures: Phase evolution and phase competition. The investigation of alloy samples subjected to heat treatments at various temperatures reveals the following phase evolutions:

At 400°C, the atomic diffusion rate increases sufficiently to enable the isothermal transformation $\beta \to \omega$, known as the ω_{iso} Transformation, which is controlled by atomic diffusion. In β -group alloys, the ω_{iso} can be formed during heat treatment. If insufficient time is available for structural ordering and long-range atomic diffusion, shear transformation or interlocking will occur instead of atomic rearrangement. The simultaneous presence of β , α' , α'' , and ω phases at this temperature indicates non-equilibrium conditions and competition between different phase transformations. The increased intensity of the α' phase compared to the hot-rolled and cold-rolled states may result from recovery and recrystallization effects at 400°C on the martensitic structure formed by rolling.

Hence, two types of omega phases have been identified:

- Athermal omega (ω_{ath}): Forms during rapid quenching (sudden cooling) from the β phase region.
- **Isothermal omega** (ω_{iso}): Can form during the aging process at relatively high temperatures (around 100 to 500°C), providing the necessary time for formation and growth.

At 700°C, the peaks of the martensitic α' and α'' phases become much weaker, while the intensity of the ω phase significantly increases. The transformation processes of martensitic phases to the ω phase $(\alpha'/\alpha'' \to \omega)$ and the direct transformation of the β phase to the ω phase $(\beta \to \omega)$ progresses with the increase in temperature from 400 to 700°C. The higher atomic diffusion rate facilitates diffusion-controlled transformations, resulting in an increased volume fraction of the ω phase and a decreased volume fraction of the martensitic phases. During heating, the ω_{ath} dissolves and transforms into the ω_{iso} phase. Controlled aging can also lead to the growth and coarsening of the ω phase, future increasing its volume fraction.

At 850°C, the proportion of the ω phase decreases slightly, while the intensity of the α' and α'' phase peaks increases. This phenomenon is complex, potentially due to competition between different phase transformations and changes in the relative phase stability with temperature. The decrease in the ω phase at this temperature may indicate greater thermodynamic instability compared to lower temperatures. The increased presence of the α' and α'' phases at 850°C may be attributed to the reverse transformation of the ω phase to the β phase ($\omega \to \beta$) followed by the

re-transformation of the β phase to martensitic phases $(\beta \to \alpha'/\alpha'')$ during cooling. The cooling rate at this temperature and the alloy composition may encourage martensitic phase formation once more. Theoretical studies suggested that the stability range of the ω phase extends above 420° C, indicating that strain energy and other factors may lover the actual onset temperature for ω phase formation. ^{70–72}

At 900 and 1000°C, the peaks of the β phase begin to increase in intensity, gradually becoming the dominant phase in the structure. This change indicates the reverse transformation $\alpha'/\alpha'' \to \beta$ at these higher temperatures. The peaks of the α'' phase increase significantly as well. At 1000°C, both the β phase and residual ω and α'' phases remain.

As temperature increases, the Gibbs free energy of the β phase decreases relative to the α' and α'' phases, facilitating the reverse phase transformation $\alpha'/\alpha'' \to \beta$. Thus, martensitic phases formed at lower temperatures revert back to the β phase at higher temperatures. However, the presence of ω and α'' phases at 1000°C suggests that complete phase equilibrium has not been achieved, indicating that these phases may exist as residuals in the structure or have reformed during cooling from 1000°C .

Factors affecting the deformation mechanism

The dominant deformation mechanism in metastable β -Ti based alloys, such as Ti-37.5Nb-4.5Zr (wt.%) alloy, are illustrated in Figure 7. These mechanisms include dislocation slip, mechanical twinning, and stress and/or strain-induced phase transformation. Dislocation slip is the primary plastic deformation mechanism, especially at higher strains, allowing dislocations to move through the crystal lattice.

SIM occurs as a result of applied stress rather than through thermal effects, leading to the formation of martensitic α' and α'' phases during deformation and mechanical loading. Factors such as grain size and strain rate significantly influence the deformation mechanism.

Research on the Schmid factor and twin formation indicates that reducing grain size complicates the formation of twins within the structure. Under conditions where the β matrix phase remains constant, increasing the strain rate shifts the deformation mechanism from martensitic transformation toward twinning. Initially, the deformation mechanism changes from exclusive martensitic transformation to a combination of martensitic transformation and twinning. At very high strain rates, however, martensitic transformation does not occur, and twinning becomes the sole mechanism for strain accommodation. 73

In the investigated alloy (Ti-37.5Nb-4.5Zr), the stability of the ω phase is present, yet the phenomenon of SIM was observed. This indicates that an interaction between the ω phase and martensitic transformation (SIM α' and SIM α'') can occur, depending on the alloy's chemical composition.

Figure 8 presents the tensile stress-strain curves of the investigated alloy in the cold-rolled state and after annealing treatments at various temperatures from 400 to 1000°C for 30 min. Also, the mechanical properties are extracted from these curves are listed in Table 2.

Based on the results presented in Table 2, the cold-rolled sample exhibits the highest values for yield strength ($1050 \pm 20 \text{ MPa}$) and tensile strength ($1350 \pm 15 \text{ MPa}$) among the

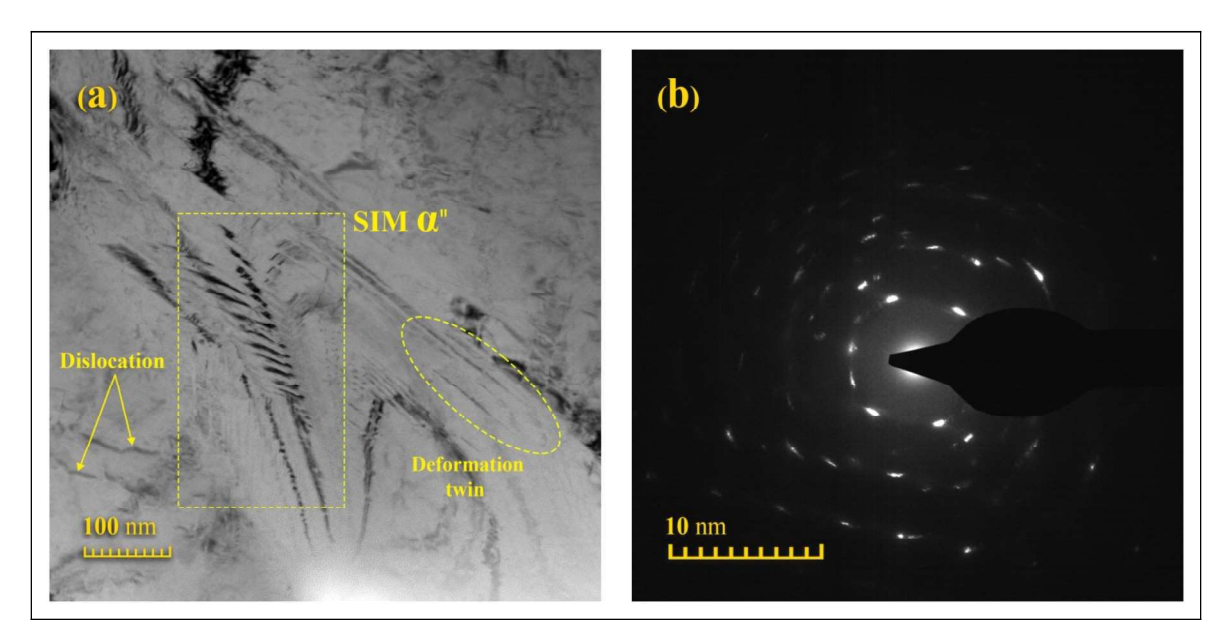


Figure 7. The BF image illustrating deformation mechanisms in cold-rolled Ti-37.5Nb-4.5Zr alloy. (a) dislocations, deformation twins, and strain-induced martensite (SIM α") phase, and (b) corresponding SAED pattern.

samples studied. This high strength can be attributed to the work-hardened structure and the increased dislocation density resulting from the cold rolling process. However, this process also leads to a reduction in ductility and toughness. The presence of strain-induced martensitic α'/α'' phases (SIM) in the cold-rolled structure likely plays a significant role in enhancing its strength.

In examining the heat-treated samples, a temperature of 400°C leads to a remarkable increase in hardness $(320 \pm 11 \, \text{HV})$, achieving the highest hardness value among all samples. This increase is likely due to the formation of the ω_{iso} phase during heat treatment at this temperature, as the ω phase is inherently hard and contributes to the alloy's hardness. Compared to the cold-rolled sample, a slight decrease in yield and tensile strength is observed at 400°C , which may be attributed to a reduction in dislocation density (recovery) during heat treatment. Despite this, the overall strength remains high, owing to the hardening effect of the ω phase and the possible presence of residual martensitic phases. The slight increase in toughness at this temperature may suggest a moderation of the work-hardened structure and a reduction in internal stresses.

At 500°C, the tensile strength and the yield strength significantly decrease to 700 ± 15 and 1080 ± 30 MPa, while elongation remains low (2.7%) and toughness is similar to that in the cold-rolled state (25 MJ/m³). The elastic modulus and hardness show a slight decrease compared to 400° C. These changes could be attributed to the ongoing growth and coarsening of the ω phase and the possible onset of ω phase instability. The decrease in tensile strength may indicate the beginning of the $\omega \to \beta$ transformation or changes in the morphology of the ω phase, resulting in reduced strength. The persistently low elongation and toughness further confirm the embrittlement effect of the ω phase.

At 600°C, there is a marked decrease in both yield and tensile strength (600 \pm 10 and 930 \pm 25 MPa, respectively). However, elongation shows a slight improvement (9.9 \pm 0.3%), and toughness significantly increases to 87 \pm 3 MJ/m³. This change

in mechanical behavior is likely due to considerable progress of the $\omega \to \beta$ transformation at this temperature. The reduction in the volume fraction of the hard ω phase and the increase presence of the softer β phase in the matrix contribute to the decreased strength and hardness, while enhancing ductility and toughness.

At 700°C, significant changes in mechanical properties are observed. The elongation increases dramatically (26.2 \pm 1.1%), reaching its highest value among the tested samples, and toughness also improves significantly, reaching its maximum value of 251 ± 8 MJ/m³. This suggests that at 700°C, the phase equilibrium shifts, allowing the β phase to becomes dominant, with fine, dispersed ω phase precipitates optimally distributed in the matrix. This ideal microstructure provides an exceptional balance of strength and ductility, resulting in high toughness. The increase in elongation demonstrates a significant improvement in flexibility under these conditions. At this temperature, both thermal and isothermal ω phases likely form during heat treatment, and controlled aging may facilitate the growth of the ω phase, while preventing excessive embrittlement from its accumulation.

At temperatures higher than 700°C, the stability of the β phase increasingly dominates, leading to gradual decomposition of the ω phase. At 900 and 1000°C, the peaks of the β phase intensify, progressively become the dominant phase in the structure. The reverse phase transformation $(\alpha'/\alpha'' \to \beta)$ occurs in this temperature range. The structure tends towards a predominantly single β phase with coarser grains, generally leads to a decrease in strength and hardness, with irregular changes in elongation and toughness. At 1000°C, although the β phase remains dominant, some amounts of the ω and α'' phases are still stable within the structure. This indicates that complete phase equilibrium has not fully shifted towards the β phase at this temperature and cooling rate, with ω and α'' phases likely being present as residuals or have reformed during final cooling.

According to Figure 8, at 700°C, there is a significant improvement in elongation $(26.2 \pm 1.1\%)$ and toughness

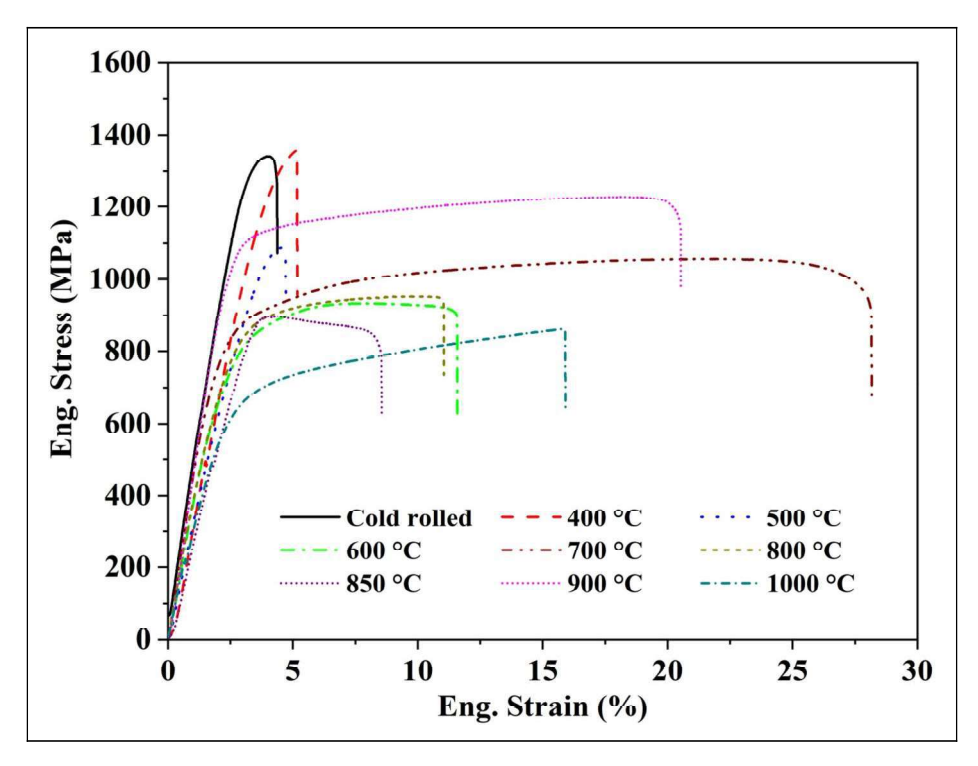


Figure 8. Tensile stress-strain curves of the Ti-37.5Nb-4.5Zr alloy in the cold-rolled state and after solution heat treatment at various temperatures from 400 to 1000°C for 30 min.

Table 2. Mechanical properties of the Ti-37.5Nb-4.5Zr (wt.%) alloy under various processing conditions.

Sample	Yield strength (MPa)	Tensile strength (MPa)	Elongation (%)	Elastic modulus (GPa)	Hardness (HV)	δ (%)	Toughness (MJ/m³)
Cold rolled	1050 ± 20	1350 ± 15	2.1 ± 0.2	40.5 ± 0.2	233 ± 8	2.6 ± 0.1	25 ± 2
400°C, 30 min	1000 ± 15	1340 ± 20	2.4 ± 0.3	35.6 ± 0.3	320 ± 11	2.8 ± 0.1	26 ± I
500°C, 30 min	700 ± 15	1080 ± 30	2.7 ± 0.4	29.6 ± 2.1	224 ± 7	2.4 ± 0.2	25 ± 2
600°C, 30 min	600 ± 10	930 ± 25	9.9 ± 0.3	36.5 <u>+</u> 1.1	191 ± 5	1.5 ± 0.2	87 ± 3
700°C, 30 min	750 ± 10	1050 ± 10	26.2 ± 1.1	44 ± 0.4	243 ± 7	1.7 ± 0.1	251 ± 8
800°C, 30 min	650 ± 25	950 ± 25	9.0 ± 1.0	37.1 \pm 0.9	229 ± 6	1.8 ± 0.1	83 ± 3
850°C, 30 min	800 ± 10	900 ± 5	5.0 ± 0.5	27.0 ± 0.6	221 ± 6	2.9 ± 0.2	48 ± 2
900°C, 30 min	970 ± 30	1230 ± 10	17.9 ± 0.2	47.9 ± 2.1	252 ± 8	2.2 ± 0.1	220 ± 5
1000°C, 30 min	540 ± 20	860 ± 5	14 <u>+</u> 0.3	26.9 ± 0.8	295 ± 8	1.8 <u>+</u> 0.1	120 ± 10

(over 250 MJ/m³), while the strength remains at an acceptable level. The stress-strain curve exhibits extensive plastic behavior, suggesting that 700°C is the optimal temperature for achieving a balance between strength and ductility in this alloy.

At this temperature, the β phase most likely becomes the dominant phase, with fine, dispersed ω phase precipitates optimally distributed in the matrix. This ideal microstructure facilitates the simultaneous activation of dislocation slip and TWIP/TRIP mechanisms, enhancing both strength and ductility. The critical role of twinning (particularly {112} twinning) and strain-induced martensitic transformation (SIMT) in increasing strain hardening and uniform elongation is essential for interpreting this behavior. ^{72,73,76–79}

Furthermore, TEM analysis, as shown in Figure 9(a), along with similar studies, reveals that under deformation, nanoscale and microscale secondary {112} twins form within the primary {112} twins. In Figure 9(b), with higher magnification, we observe dislocation pile-ups and

dislocation slips alongside the primary twins. SAED patterns presented in Figures 9(c) & (d) clearly demonstrate the aforementioned points, and in Figure 9(e), a hierarchical structure consisting of primary, secondary, and ternary twins is formed, which contributes to the TWIP effect.

These {112} twinning structures, similar to {332} twinning, act as obstacles to dislocation motion. This obstruction makes dislocation movement move challenging, resulting in increased hardness and resistance to deformation due to a higher strain hardening rate. While {112} twinning hinders dislocation motion, it also helps prevent premature fracture by distributing stress more uniformly throughout the metal, thereby reducing stress concentration and the likelihood of crack initiation. Consequently, the metal exhibits improved ductility. ^{80–82}

The high formation of $\{112\}$ twinning structures is similar to refining metal grains. According to the Hall-Petch effect, finer grains contribute to increased strength in metals. Therefore, $\{112\}$ twinning also plays a role in strengthening the alloy. $^{80-82}$

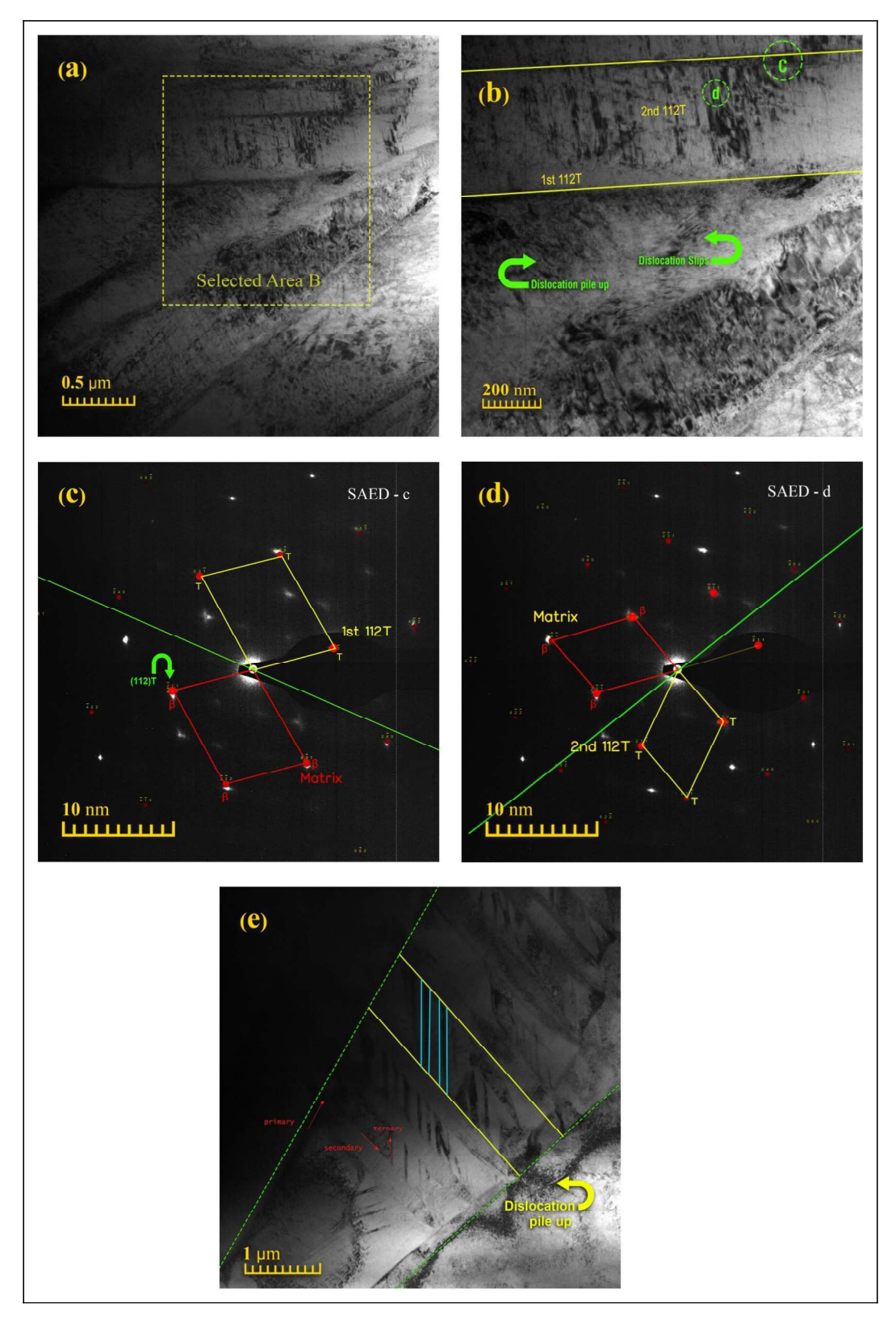


Figure 9. TEM micrographs of the Ti-37.5Nb-4.5Zr alloy annealed at 700° C: (a) BF image of 112 T bands (low magnification); (b) close-up BF image of selected-area in (a); (c, d) the corresponding SAED patterns of selected-area in (b) labeled c and d with white dotted cycles, along the zone axis (ZA) [102] β ; (e) the TEM micrograph of the sample annealed at 700° C sample showing the hierarchical twinned structures.

As dislocations interact with {112} twinning structures, these boundaries act as barriers to dislocation motion, causing dislocations to accumulate and further hardening the metal. However, pathways within the {112} twinning structures facilitate dislocation movement, allowing for controlled

dislocation motion and preventing accumulation that could lead to fracture. 70,73,80-82

The innovative approach in designing the Ti-37.5 Nb-4.5Zr (wt.%) alloy involves combining ω_{iso} precipitation with the mechanisms of TWIP and TRIP to address the issue

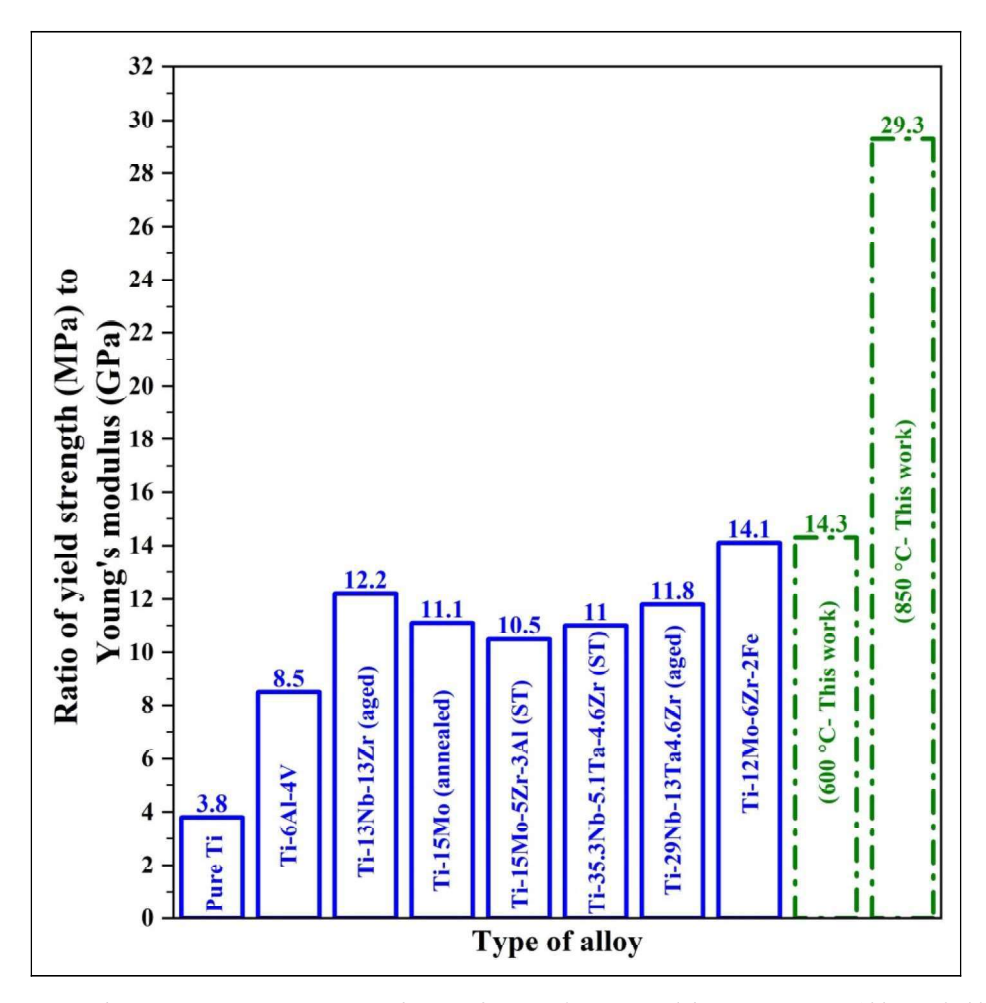


Figure 10. Comparison of strength-to-modulus ratios of the Ti-37.5Nb-4.5Zr alloy (after annealing at 600 and 850°C) with various typical implant materials.

of reduced ductility. When these mechanisms work together, their result obtained is better than the simple sum of each individual effect. That is, their synergistic effect exceeds the simple sum of their individual contributions. 12,76,79

During the early stages of aging at low temperatures, Nb segregation mediates the precipitation of the ω_{iso} phase, influencing active deformation mechanisms (mechanical twinning {112}, martensitic transformation $\beta \to \alpha''$, and dislocation slip). Although the precipitation of the ω phase gradually suppresses these deformation mechanisms, {112} twinning demonstrates considerable resistance to the ω phase formation.

In this alloy, the TRIP and TWIP mechanisms operate collaboratively. The phase transformation can create internal stresses that promote twinning, making the activation of twinning easier. Once the phase transformation reaches a certain point, twinning can serve as an additional deformation mechanism, allowing the alloy to continue deforming while maintaining strength and ductility. ^{12,76,79}

Ratio of strength-to-Young's modulus

For titanium alloys intended for biomedical applications, particularly bone implants, achieving a low Young's modulus is critically important. Investigations have elucidated that the reduction of Young's modulus in these alloys is intrinsically linked to the stabilization of the metastable β phase and the

phenomenon of SIM transformation. Additionally, lattice expansion from the incorporation of elements like Nb further contributes to this modulus reduction.

The presence of a limited fraction of α " martensite, alongside its detwinning reorientation mechanisms, also significantly influences the reduction of Young's modulus. As illustrated in Figure 10, the β Ti-37.5Nb-4.5Zr alloy exhibits excellent performance, with a strength-to-modulus ratio of approximately 1.4 and 2.9% after annealing at 600 and 850°C, respectively.

This alloy emerges as a promising material for biomedical implants, as the strength-to-modulus ratio is a crucial metric for evaluating material efficacy in bone implant applications.

Such favorable characteristics are readily achieved by metastable β titanium alloys with a refined microstructure, typically characterized by fine grains, densely distributed dislocations, and α phase precipitates. These features work synergistically to contribute to the desired property profile. ^{83,84}

Conclusions

This research addresses the critical need for advanced biomaterials by focusing on the design of a novel Ti-37.5Nb-4.5Zr alloy tailored for orthopedic implant applications. The primary objectives included overcoming the inherent strength-ductility trade-off characteristic of titanium alloys and

minimizing stress shielding through the achieving a low Young's modulus. The main findings are

- A 75% reduction in hot rolling and a 95% reduction in cold rolling demonstrated the excellent formability of this alloy.
- The alloy design capitalized on the principles of metastable β -Ti alloys, incorporating TRIP/TWIP mechanisms and controlled phase transformations (β , ω , α' , and α'') to achieve an optimal balance of mechanical properties.
- Mechanisms of dislocation slip, TRIP, and TWIP were investigated across all samples, with dislocation slip acting as the predominant deformation mechanism.
- The TWIP/TRIP effect was more pronounced in the sample annealed at 700°C, which exhibited the most superior combination of mechanical properties. This was attributed to the synergistic effects of ω phase precipitation strengthening and the harmonious interaction of the TWIP/TRIP mechanisms.
- The best strength-to-modulus ratio ($\delta = 1.4-2.9\%$) in the annealed samples reflects a very promising performance compared to many of the materials studied.
- The lowest elastic modulus, ~27 GPa, was observed in the samples annealed at 850 and 1000 °C.

ORCID iD

Saeed Hasani https://orcid.org/0000-0001-7093-8262

Ethics approval

Not applicable.

Consent for publication

We confirm that this manuscript presents original research and is not currently under consideration for publication elsewhere. All authors have reviewed and approved the submission of this manuscript and agree to transfer the copyright to Metals and Materials International upon acceptance.

Consent to participate

All participants in this study provided informed consent after receiving comprehensive information about the research objectives, methodologies, potential benefits, and risks. The consent form explicitly stated their right to withdraw from the study at any stage without facing adverse consequences.

Author contribution(s)

Arash Etemad: Data curation; Formal analysis; Investigation; Resources; Software; Writing – original draft.

Alireza Mashreghi: Formal analysis; Methodology; Supervision; Validation; Writing – review & editing.

Saeed Hasani: Conceptualization; Formal analysis; Methodology; Project administration; Supervision; Validation; Writing – review & editing.

Sabine Schwarz: Data curation; Formal analysis; Resources; Software; Visualization; Writing – review & editing.

Martin Lombaard: Formal analysis; Investigation; Resources; Writing – review & editing.

Funding

The authors received no financial support for the research, authorship, and/or publication of this article.

Declaration of conflicting interests

The authors declared no potential conflicts of interest with respect to the research, authorship, and/or publication of this article.

Availability of data and material

Data will be made available on request.

Declaration of generative Al and Al-assisted technologies in the writing process

During the preparation of this work, the authors used Chatgpt 3.5 of openAI in order to refine language and improve readability. After using this tool, the authors reviewed and edited the content as needed and take full responsibility for the content of the publication.

Code availability

Not applicable.

References

- 1. Semiatin SL. An overview of the thermomechanical processing of α/β Titanium alloys: current Status and future research opportunities. *Metall Mater Trans A* 2020; 51: 2593–2625.
- 2. Cao MZ and He BB. A review on deformation mechanisms of metastable β titanium alloys. *J Mater Sci* 2024; 59: 14981–15016.
- 3. Biesiekierski A, Lin J, Munir K, et al. An investigation of the mechanical and microstructural evolution of a TiNbZr alloy with varied ageing time. *Sci Rep* 2018; 8: 5737.
- Abdel-Hady Gepreel M and Niinomi M. Biocompatibility of Ti-alloys for long-term implantation. *J Mech Behav Biomed Mater* 2013; 20: 407–415.
- Fu Y, Wang J, Xiao W, et al. Microstructure evolution and mechanical properties of ti–8Nb–2Fe-0.2O alloy with high elastic admissible strain for orthopedic implant applications. *Prog Nat Sci Mater Int* 2020; 30: 100–105.
- 6. Bahl S, Suwas S and Chatterjee K. Comprehensive review on alloy design, processing, and performance of β Titanium alloys as biomedical materials. *Int Mater Rev* 2021; 66: 114–139.
- 7. Kolli RP and Devaraj A. A review of metastable Beta Titanium alloys. *Metals (Basel)* 2018; 8: 06.
- 8. Gupta A, Khatirkar R and Singh J. A review of microstructure and texture evolution during plastic deformation and heat treatment of β-ti alloys. *J Alloys Compd* 2022; 899: 163242.
- 9. Cotton JD, Briggs RD, Boyer RR, et al. State of the art in Beta Titanium alloys for airframe applications. *JOM* 2015; 67: 1281–1303.
- 10. Chen L-Y, Cui Y-W and Zhang L-C. Recent development in Beta Titanium alloys for biomedical applications. *Metals* (*Basel*) 2020; 10: 1139.
- 11. Lai MJ, Li T and Raabe D. Ω phase acts as a switch between dislocation channeling and joint twinning- and transformation-induced plasticity in a metastable β titanium alloy. *Acta Mater* 2018; 151: 67–77.
- 12. Tang J, Yang H, Qian B, et al. TWIP-assisted Zralloys for medical applications: design strategy, mechanical properties and first biocompatibility assessment. *J Mater Sci Technol* 2024; 184: 32–42.

- Etemad A, Dini G and Schwarz S. Accumulative roll bonding (ARB)-processed high-manganese twinning induced plasticity (TWIP) steel with extraordinary strength and reasonable ductility. *Mater Sci Eng A* 2019; 742: 27–32.
- Fu Y, Gao Y, Jiang W, et al. A review of deformation mechanisms, compositional design, and development of Titanium alloys with transformation-induced plasticity and twinninginduced plasticity effects. *Metals (Basel)* 2024; 14: 97.
- 15. Pang EL, Pickering EJ, Baik SI, et al. The effect of zirconium on the omega phase in Ti-24Nb-[0–8]zr (at.%) alloys. *Acta Mater* 2018; 153: 62–70.
- 16. Sun J. Examination of α' , α' and ω phases in a β -type titanium–niobium metal. *Mater Test* 2022; 64: 1720–1732.
- Kolli RP, Joost WJ and Ankem S. Phase stability and stress-induced transformations in Beta Titanium alloys. *JOM* 2015; 67: 1273–1280.
- Hanada S and Izumi O. Deformation of metastable betaTi-15Mo-5Zr alloy single crystals. *Metall Trans A* 1980; 11: 1447–1452.
- Hanada S and Izumi O. Correlation of tensile properties, deformation modes, and phase stability in commercial β-phase titanium alloys. *Metall Trans A* 1987; 18: 265–271.
- Furuhara T, Takagi S, Watanabe H, et al. Crystallography of grain boundary α precipitates in a β titanium alloy. *Metall Mater Trans A* 1996; 27: 1635–1646.
- 21. Hanada S, Ozeki M and Izumi O. Deformation characteristics in B phase Ti-Nb alloys. *Metall Trans A* 1985; 16: 789–795.
- Min X, Chen X, Emura S, et al. Mechanism of twinning-induced plasticity in β-type Ti–15Mo alloy. Scr Mater 2013; 69: 393–396.
- Neelakantan S, Rivera-Díaz-del-Castillo PEJ and van der Zwaag S. Prediction of the martensite start temperature for β titanium alloys as a function of composition. Scr Mater 2009; 60: 611–614.
- 24. Welsch G, Boyer R and Collings EW. *Materials Properties Handbook: Titanium Alloys*. Materials Park, OH, USA: ASM International, 1994.
- 25. Abdel-Hady M, Hinoshita K and Morinaga M. General approach to phase stability and elastic properties of β-type Ti-alloys using electronic parameters. *Scr Mater* 2006; 55: 477–480.
- 26. Kuroda D, Niinomi M, Morinaga M, et al. Design and mechanical properties of new β type titanium alloys for implant materials. *Mater Sci Eng A* 1998; 243: 244–249.
- 27. Ehtemam-Haghighi S, Prashanth KG, Attar H, et al. Evaluation of mechanical and wear properties of Ti xNb 7Fe alloys designed for biomedical applications. *Mater Des* 2016; 111: 592–599.
- 28. Wang CH, Russell AM and Cao GH. A semi-empirical approach to the prediction of deformation behaviors of β-Ti alloys. *Scr Mater* 2019; 158: 62–65.
- 29. Morinaga M, Yukawa N, Maya T, et al. in *Sixth world conference on titanium*. *III*, 1998, pp. 1601–6.
- 30. Dai N, Zhang L-C, Zhang J, et al. Distinction in corrosion resistance of selective laser melted Ti-6Al-4V alloy on different planes. *Corros Sci* 2016; 111: 703–710.
- 31. Saito T, Furuta T, Hwang J-H, et al. Multifunctional alloys obtained via a dislocation-free plastic deformation mechanism. *Science* (80-) 2003; 300: 464–467.
- 32. Withey E, Jin M, Minor A, et al. The deformation of "gum metal" in nanoindentation. *Mater Sci Eng A* 2008; 493: 26–32.

- 33. Hao YL, Li SJ, Sun SY, et al. Elastic deformation behaviour of Ti–24Nb–4Zr–7.9Sn for biomedical applications. *Acta Biomater* 2007; 3: 277–286.
- 34. Ikehata H, Nagasako N, Furuta T, et al. First-principles calculations for development of low elastic modulus Ti alloys. *Phys Rev B* 2004; 70: 174113.
- 35. Tane M, Nakano T, Kuramoto S, et al. Low young's modulus in Ti–Nb–Ta–Zr–O alloys: cold working and oxygen effects. *Acta Mater* 2011; 59: 6975–6988.
- 36. Hwang J, Kuramoto S, Furuta T, et al. Phase-Stability dependence of plastic deformation behavior in Ti-Nb-Ta-Zr-O alloys. *J Mater Eng Perform* 2005; 14: 747–754.
- 37. Marteleur M, Sun F, Gloriant T, et al. On the design of new β-metastable titanium alloys with improved work hardening rate thanks to simultaneous TRIP and TWIP effects. *Scr Mater* 2012; 66: 749–752.
- 38. Gabor C, Cristea D, Velicu I-L, et al. Ti–Zr–Si–Nb nanocrystalline alloys and metallic glasses: assessment on the structure, thermal stability, corrosion and mechanical properties. *Materials (Basel)* 2019; 12: 1551.
- 39. Samiee A, Casillas G, Ahmed M, et al. 2018.
- 40. Nonato RBP and Restivo TAG. vol. 9, Editora Conhecimento Livre, 2022.
- 41. Mazur AV, Gasik MM and Mazur VI. Study of Ti–Si in situ composite processing by multi-stage eutectic solidification. *Int J Mater Res* 2022; 95: 377–380.
- 42. Ukabhai K, Nape K, Spotose L, et al. Thermo-mechanical processing and phase analysis of titanium alloys with copper additions. *Suid-Afrikaanse Tydskr vir Natuurwetenskap en Tegnol* 2021; 40: 84–90.
- 43. Kuroda PAB, Lourenço ML, Correa DRN, et al. Thermomechanical treatments influence on the phase composition, microstructure, and selected mechanical properties of Ti–20Zr–Mo alloys system for biomedical applications. J Alloys Compd 2020; 812: 152108.
- 44. Kim KM, Kim HY and Miyazaki S. Effect of Zr content on phase stability, deformation behavior, and Young's modulus in Ti–Nb–Zr alloys. *Materials (Basel)* 2020; 13: 76.
- 45. Acharya S, Panicker AG, Laxmi DV, et al. Study of the influence of zr on the mechanical properties and functional response of Ti-Nb-Ta-Zr-O alloy for orthopedic applications. *Mater Des* 2019; 164: 107555.
- 46. Elshaer RN, Ibrahim KM, Barakat AF, et al. Determination of phase transformation for TC21 Ti-alloy by dilatometry method. *Open J Met* 2019; 09: 1–10.
- 47. Sun B, Meng XL, Gao ZY, et al. Martensitic transformation and shape memory effect of Ti–16Nb–xZr (x = 0–8) alloys. *Phys Met Metallogr* 2019; 120: 750–755.
- 48. Talbot C, Church N, Hildyard E, et al. On the stability and formation of the α'' and ω phases in Ti-Nb alloys upon cooling. *Acta Mater* 2024; 262: 119409.
- Veverková A, Harcuba P, Veselý J, et al. Sequence of phase transformations in metastable β Zr–12Nb alloy studied in situ by HEXRD and complementary techniques. *J Mater Res Technol* 2023; 23: 5260–5269.
- 50. Brumbauer F, Okamoto NL, Ichitsubo T, et al. Minor additions of Sn suppress the omega phase formation in beta titanium alloys. *Acta Mater* 2024; 262: 119466.
- Li Y, Zhou L, Lin J, et al. Phase transformation behavior and kinetics of high Nb–TiAl alloy during continuous cooling. J Alloys Compd 2016; 668: 22–26.

- 52. Qiu RS, Luan BF, Chai LJ, et al. Effects of heating rates and alloying elements (Sn, Cu and Cr) on the $\alpha \rightarrow \alpha + \beta$ phase transformation of Zr–Sn–Nb–Fe–(Cu, Cr) alloys. *J Nucl Mater* 2014; 453: 269–274.
- 53. Dubinskiy SM, Baranova AP and Brailovski V. *Izv. Vuzov. Tsvetnaya Metall.* (Universities' Proc. Non-Ferrous Metall., 2022, pp. 78–84.
- Zháňal P, Harcuba P, Hájek M, et al. Evolution of ω phase during heating of metastable β titanium alloy Ti–15Mo. *J Mater Sci* 2018; 53: 837–845.
- Pang EL, Hildyard EM, Connor LD, et al. The effect of quench rate on the β-α" martensitic transformation in Ti–Nb alloys. Mater Sci Eng A 2021; 817: 141240.
- Choi SH, Ali B, Choi KS, et al. Reaction kinetics and morphological study of TiNb2O7 synthesized by solid-state reaction. *Arch Metall Mater* 2017; 62: 1051–1056.
- Lada P, Miazga A, Bazarnik P, et al. Zirconia—Titanium interface in ceramic based composite. *Powder Metall Met Ceram* 2018; 57: 458–464.
- Si K, Wang X, Yin Z, et al. Influence of oxygen and zirconium contents on the mechanical properties of Ti-23Nb-0.7Ta-Zr-O alloys. *Metals (Basel)* 2022; 12: 1018.
- Hoppe V, Szymczyk-Ziółkowska P, Rusińska M, et al. Assessment of mechanical, chemical, and biological properties of Ti-Nb-Zr alloy for medical applications. *Materials (Basel)* 2020: 14: 26.
- Lai W, Zhao X, Yi Y, et al. Effect of phase decomposition on the mechanical properties of Ti-Zr-Nb-Ta-Mo multi-principal element alloys. *J Mater Sci Technol* 2024; 199: 206–221.
- Lee T. Variation in mechanical properties of Ti-13Nb-13Zr depending on annealing temperature. *Appl Sci/3192* 2020; 10: 7896.
- 62. de Fontaine D. Simple models for the omega phase transformation. *Metall Trans A* 1988; 19: 169–175.
- 63. Arul Kumar M, Hilairet N, McCabe RJ, et al. Role of twinning on the omega-phase transformation and stability in zirconium. *Acta Mater* 2020; 185: 211–217.
- 64. Ballor J, Li T, Prima F, et al. A review of the metastable omega phase in beta titanium alloys: the phase transformation mechanisms and its effect on mechanical properties. *Int Mater Rev* 2023; 68: 26–45.
- Rabadia CD, Liu YJ, Zhao CH, et al. Improved trade-off between strength and plasticity in titanium based metastable beta type Ti-Zr-Fe-Sn alloys. *Mater Sci Eng A* 2019; 766: 138340.
- Jawed SF, Rabadia CD, Liu YJ, et al. Beta-type Ti-Nb-Zr-Cr alloys with large plasticity and significant strain hardening. *Mater Des* 2019; 181: 108064.
- 67. Mamivand M, Zaeem MA and El Kadiri H. A review on phase field modeling of martensitic phase transformation. *Comput Mater Sci* 2013; 77: 304–311.
- 68. Daly S, Ravichandran G and Bhattacharya K. Stress-induced martensitic phase transformation in thin sheets of Nitinol. *Acta Mater* 2007; 55: 3593–3600.

69. Chilnicean G-A, Sprâncenatu R, Zhao X, et al. in *AIP Conference Proceedings*, AIP Publishing, 2017, p. 040008.

- Josephine Prabha A, Raju S, Jeyaganesh B, et al. Thermodynamics of α"→β phase transformation and heat capacity measurements in Ti–15at% Nb alloy. *Phys B Condens Matter* 2011; 406: 4200–4209.
- Wang XL, Li L, Mei W, et al. Dependence of stress-induced omega transition and mechanical twinning on phase stability in metastable β Ti–V alloys. *Mater Charact* 2015; 107: 149–155.
- 72. Zhang J, Qian B, Lin W, et al. Compressive deformation-induced hierarchical microstructure in a TWIP β Ti-alloy. *J Mater Sci Technol* 2022; 112: 130–137.
- 73. Tang J, Zorgati A, Gaillard J-B, et al. Twinning-induced plasticity (TWIP) effect in multi-phase metastable beta Zr-Nb alloys. *J Mater Sci Technol* 2023; 139: 120–125.
- Nartu MSKKY, Sharma A, Mantri SA, et al. Increasing the yield strength while preserving strain hardenability and ductility in a beta titanium alloy exhibiting transformation induced plasticity (TRIP). Scr Mater 2022; 219: 114890.
- Qian B, Mantri SA, Dasari S, et al. Mechanisms underlying enhanced strength-ductility combinations in TRIP/TWIP Ti-12Mo alloy engineered via isothermal omega precipitation. *Acta Mater* 2023; 245: 118619.
- 76. Yang Y, Li GP, Wang H, et al. Formation of zigzag-shaped $\{1\ 1\ 2\}\ \langle 1\ 1\ 1\rangle\ \beta$ mechanical twins in Ti–24.5 Nb–0.7 Ta–2 Zr–1.4 O alloy. *Scr Mater* 2012; 66: 211–214.
- Prima F, Vermaut P, Texier G, et al. Evidence of α-nanophase heterogeneous nucleation from ω particles in a β-metastable Ti-based alloy by high-resolution electron microscopy. Scr Mater 2006; 54: 645–648.
- Ellyson B, Klemm-Toole J, Clarke K, et al. Tuning the strength and ductility balance of a TRIP titanium alloy. Scr Mater 2021; 194: 113641.
- Feng T, Pan Z, Li N, et al. Achieving an excellent combination of strength and ductility in metastable β titanium alloys via coupling isothermal ω phase and TRIP/TWIP effects. *Mater Charact* 2024; 218: 114531.
- 80. Qiang M, Yang X, Liu X, et al. Enhanced yield stress and reduced elastic modulus of metastable β Ti–Nb alloys deformed by equal channel angular pressing attributed to the synergistic effect of deformation mechanisms. *Mater Sci Eng A* 2024; 909: 146858.
- 81. Bertrand E, Castany P, Yang Y, et al. Origin of {112} 111 antitwinning in a Ti-24Nb-4Zr-8Sn superelastic single crystal. *J Mater Sci* 2022; 57: 7327–7342.
- 82. Dan A, Cojocaru EM, Raducanu D, et al. {332}<113> and {112}111 twin variant activation during cold-rolling of a Ti-Nb-Zr-Ta-Sn-Fe alloy. *Materials (Basel)* 2022; 15: 6932.
- 83. Liu Q, Meng Q, Guo S, et al. A' type Ti–Nb–Zr alloys with ultra-low Young's modulus and high strength. *Prog Nat Sci Mater Int* 2013; 23: 562–565.
- Matsumoto H, Watanabe S and Hanada S. Microstructures and mechanical properties of metastable β TiNbSn alloys cold rolled and heat treated. *J Alloys Compd* 2007; 439: 146–155.